Reaching High Poloidal Beta at Greenwald Density with Internal Transport Barrier Close to Full Noninductive Current Drive

J. Hobirk,[1] R. C. Wolf,[1] O. Gruber,[1] A. Gude,[1] S. Günter,[1] B. Kurzan,[1] M. Maraschek,[1] P. J. McCarthy,[2] H. Meister,[1] A. G. Peeters,[1] G. V. Pereverzev,[1] J. Stober,[1] W. Treutterer,[1] and ASDEX Upgrade Team[1]

[1]*Max-Planck-Institut für Plasmaphysik, EURATOM Association, Boltzmannstrasse 2, D-85748 Garching, Germany*

[2]*Physics Department, University College Cork, Association Euratom-DCU, Cork, Ireland*

(Received 16 April 2001; published 2 August 2001)

In the ASDEX Upgrade tokamak, high poloidal beta up to $\beta_{\rm pol} = 3$ at the Greenwald density with *H*-mode confinement has been reached. Because of the high beta, the plasma current is driven almost fully noninductively, consisting of 51% bootstrap and 43% neutral beam driven current. To reach these conditions the discharge is operated at low plasma current ($I_P = 400$ kA) and high neutral beam heating power ($P_{\rm NBI} = 10$ MW). The discharge combines an edge (*H* mode) and internal transport barrier at high densities without confinement-limiting MHD activities. The extrapolation to higher plasma currents may offer a promising way for an advanced scenario based fusion reactor.

DOI: 10.1103/PhysRevLett.87.085002 PACS numbers: 52.55.Fa

To date many tokamak discharge scenarios with an energy confinement higher than *L* mode (low-confinement mode) have been found. The *H*- or high-confinement mode was discovered [1] which is now the standard operating regime for divertor tokamaks. It is characterized by a high energy confinement time (factor of 2 larger than in *L* mode) brought about by an edge transport barrier. The steep pressure gradients associated with this transport barrier are usually limited by edge localized modes (ELMs). More recently other types of improved confinement modes have been found. The radiative improved or *RI* mode [2] combines an *L*-mode edge with raised core confinement and density near the Greenwald density [3] ($\bar{n}_e \approx n^{\rm gr}$, where $n^{\rm gr}[10^{20}\ {\rm m}^{-3}]$ is defined as $\frac{I_P}{\pi a^2}$ with a[m] minor plasma radius, I_P[MA] the plasma current, and $\bar{n}_e$ the line averaged electron density) which is generated by impurity seeding at the plasma edge. Besides these, regimes have been found with low or negative magnetic shear, mostly produced by auxiliary heating at low density during the initial current ramp of the tokamak discharge to facilitate the formation of internal transport barriers (ITBs). They generally show high ion or electron temperatures and, due to the strong pressure gradients at the ITB location, large bootstrap current fractions are driven [4–8]. Up to now, however, these ITB plasmas have several drawbacks, namely, (i) a susceptibility to confinement-limiting MHD instabilities which are caused by a lack of current and pressure profile control both in the core and at the edge of the plasma and (ii) the low electron density. Without sufficient external current drive this is aggravated by the relaxation of the current profile, in particular, at high q values. Another type of improved confinement scenario offers the prospect of stationary operation [9,10] at high normalized beta ($\beta_N = \beta_{\rm tor}/(I_p/aB_T)$ with B_T being the toroidal magnetic field), but also suffers from relatively low densities which are far below the value required in a fusion reactor. In these discharges the q profile is monotonic with low shear in the central region. Fish-bone driven reconnection with $q_0 \approx 1$ is assumed to prevent sawtooth activity, which is the main difference to a low density *H* mode.

Apart from the high energy confinement, the other important aim of an advanced tokamak is to drive the current fully noninductively to avoid pulsed operation. Since it is difficult and energetically expensive to drive current by external means, such as lower hybrid [11], electron cyclotron [12], fast wave [13], or neutral beam current drive [14], the plasma current should be mostly driven by the intrinsic bootstrap current [15], in order to keep the recirculating power in a fusion reactor at a minimum. The bootstrap fraction $f_{\rm BS}$, defined as the ratio of bootstrap to total plasma current, is proportional to the poloidal beta $\beta_{\rm pol} = 2\mu_0 \frac{\langle p\rangle_A}{\langle B_{\rm pol}\rangle^2}$, where $\langle p\rangle_A$ is the poloidal cross-section averaged plasma pressure and $\langle B_{\rm pol}\rangle$ is the average poloidal magnetic field on the plasma boundary. Discharge conditions with high poloidal beta were produced at JT60-U [4,16], reaching up to $\beta_{\rm pol} \approx 3$, high *H* factors, and full noninductive current drive, but at low normalized plasma density $\bar{n}_e/n^{\rm gr} < 0.5$. Besides, the confinement of these discharges tends to be limited by MHD activity [17].

At ASDEX Upgrade similar plasma parameters as in JT60-U are employed to create high-$\beta_{\rm pol}$ discharges. A high neutral beam heating power of $P_{\rm NBI} = 10$ MW (NBI = neutral beam injection) was injected into a plasma with a low current of $I_P = 400$ kA. The low current together with a toroidal magnetic field of $B_T = 2$ T corresponds to $q_{95} = 9$. Time traces of the major plasma parameters are shown in Fig. 1. At $t = 2.6$ s, $\beta_{\rm pol} = 3$, $\beta_N = 2.7$, and a confinement improvement factor above *L* mode ($H_{89\rm P} = 1.8$), corresponding to $\beta_N H_{89\rm P} = 4.8$, have been reached. In the first trace of Fig. 1 the total plasma current and the NBI heating power are presented. The plasma current decreases from $t = 2.5$ s onward because the flux in the ohmic transformer is kept constant while it is still required to sustain the 400 kA of total

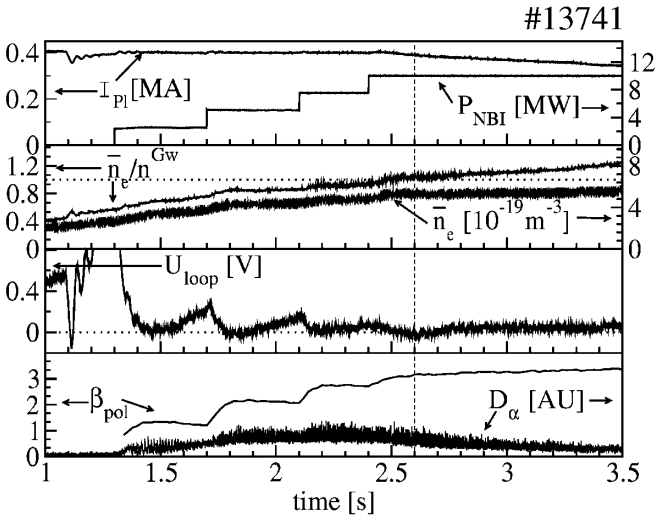

FIG. 1. Time traces of the main plasma parameters of a high-β_{pol} discharge. The upper part shows the plasma current and the neutral beam heating power. The second trace shows the line averaged density and the Greenwald factor, followed by the loop voltage. The D_α trace and the poloidal beta trace are shown at the bottom. The dashed line indicates where a more detailed analysis is done.

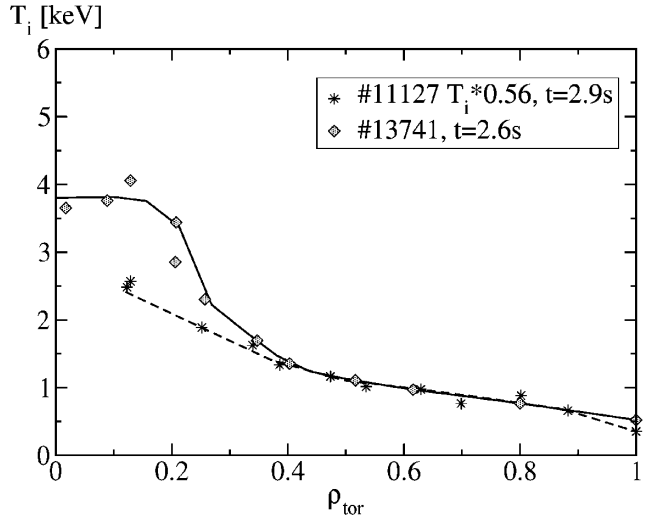

FIG. 2. The ion temperature profiles for #13741 at $t = 2.6$ s and for #11127 at $t = 2.9$ s scaled by a factor of 0.56 to be equal in the outer region of the plasma. The symbols represent the actual measured values.

plasma current. The heating power is increased in four steps of 2.5 MW to a total auxiliary heating power of 10 MW at $t = 2.4$ s. In the next part of the figure the line averaged electron density and the Greenwald factor $\bar{n}_e/n^{\mathrm{gr}}$ are shown. The density is increased by gas puffing until 2.4 s. Subsequently it is sustained at a constant level by beam fueling only above the preprogrammed value of the density feedback (natural density). The loop voltage is shown in the next trace. It decreases with additional heating power, finally reaching slightly negative values at about $t = 2.5$ s. After the flux in the Ohmic transformer is kept constant the loop voltage increases somewhat and then remains constant at a low value. In the bottom trace of Fig. 1 the edge D_α emission and the poloidal beta from the equilibrium reconstruction code CLISTE [18] using motional Stark effect (MSE) [19] measurements are presented. In the D_α emission the ELM activity can be seen from the first heating step onwards, indicating the H-mode transition. After $t = 2.5$ s the D_α emission decreases and the ELMs become less pronounced. The poloidal beta increases with every step of the NBI power up to $\beta_{\mathrm{pol}} = 3$ at $t = 2.6$ s. Subsequently it still increases, but only because the plasma current is decreasing and not due to a pressure rise. The dashed vertical line in Fig. 1 shows the time point where a more detailed data analysis is performed, as discussed below.

To show that not only an edge transport barrier in H mode but also an internal ion transport barrier has developed, in Fig. 2 the ion temperature profiles from charge exchange spectroscopy of a high-β_{pol} discharge (same as in Fig. 1) and a H-mode discharge are compared. The H-mode ion temperature profile is scaled (by a factor of 0.56) to agree with the value of the high-β_{pol} case in the outer region of the plasma. The gradient length of ion temperature profiles in ASDEX Upgrade H modes [20] is most likely limited by the ion temperature gradient (ITG) mode [21] dominated heat transport, which is associated with a fixed ratio of central to edge ion temperature [22], whereas the temperature profile in the high-β_{pol} discharge is more peaked. A clear reduction of the gradient length at $\rho_{\mathrm{tor}} \approx 0.3$ can be seen at $t = 2.6$ s, accompanied by a flattening of the profile in the plasma center, which indicates the formation of an internal transport barrier and corresponds to an increase of the ion temperature peaking factor from $T_i(0)/T_i(\rho_{\mathrm{tor}} = 0.4) = 1.8$ (H mode) to 2.9 in the high-β_{pol} discharges. A detailed analysis of the ITG mode stability is shown in Fig. 3. In the upper part the radial electric field (E_r) is displayed. The solid line represents the total E_r, consisting of the ∇p contribution (dotted line) derived from the C^{6+} impurity density and temperature and contributions from the toroidal (dash-dotted line) and the neoclassical poloidal rotation (dashed line) [23]. Here, two peculiarities should be noted, first the very low absolute value of the radial electric field and, second, the domination of the poloidal rotation in the plasma core. In ASDEX Upgrade the radial electric field is usually dominated by the toroidal rotation term [24] which is also the usual case for other experiments with strong co-NBI injection. Despite the low E_r, the large gradient of the poloidal rotation leads to a high $\vec{E} \times \vec{B}$ shearing rate, as can be seen in the lower part of Fig. 3, exceeding the linear growth rate of the ITG instability, as derived from the GLF23 model [25], over most of the plasma cross section. In this sense we assume that the transport barrier is a sign of the suppression of the ITG turbulence.

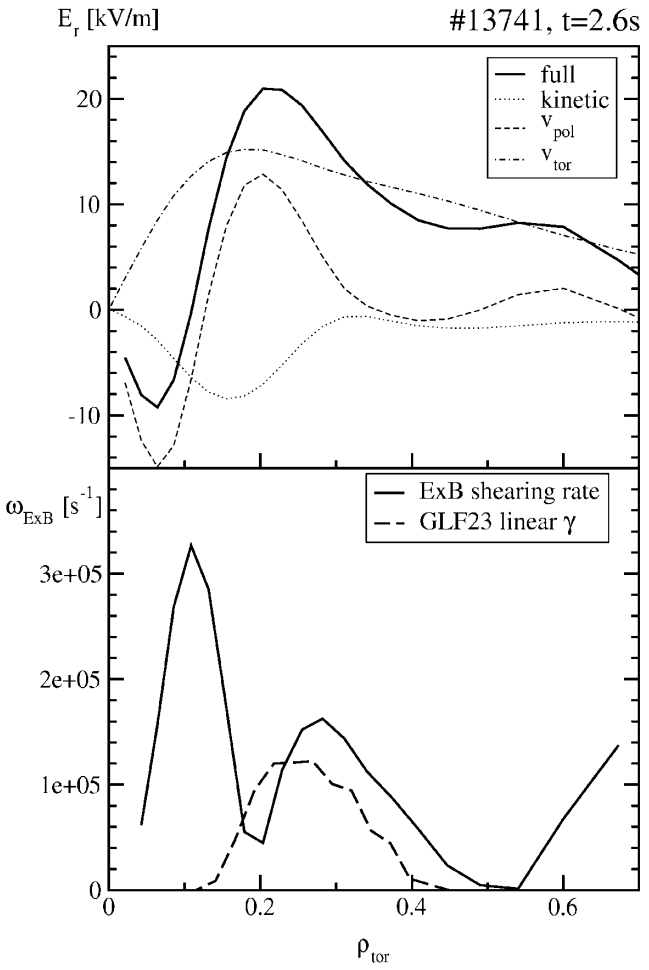

FIG. 3. Radial electric field (E_r) profile (solid line), consisting of the ∇p part (dotted line) and contributions from toroidal (dash-dotted line) and neoclassical poloidal rotation (dashed line). In the lower part of the figure the $\vec{E} \times \vec{B}$ shearing rate is compared with the linear growth rate from the GLF23 model (dashed line).

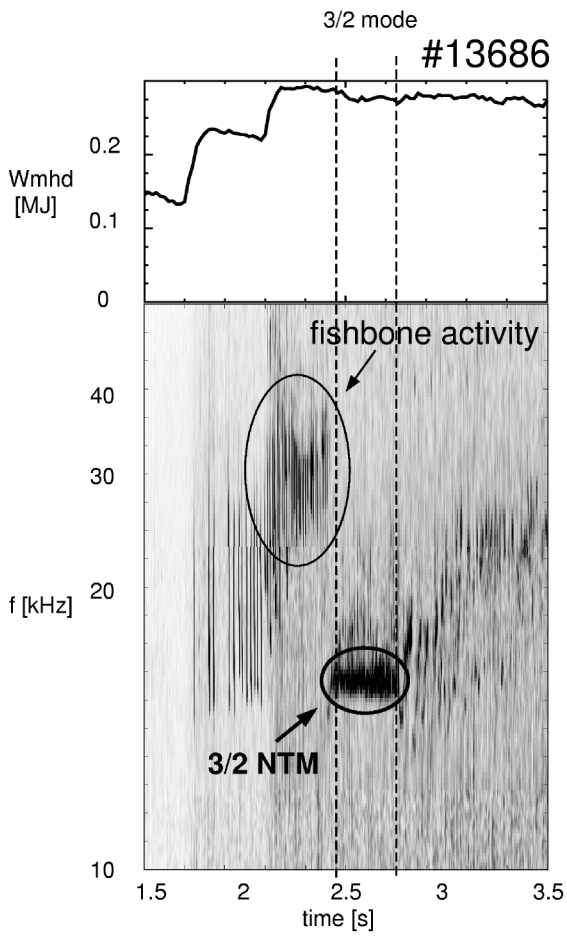

FIG. 4. In the upper part of the figure the plasma energy is plotted and the occurrence of a $3/2$ neoclassical tearing mode is marked with vertical lines. In the lower part of the figure a wavelet analysis of a magnetic probe data is presented. The fish-bone activity (about 30 kHz) and a $3/2$ neoclassical tearing mode are marked.

A critical point for discharges with high normalized β and low rational q values is its limitation due to neoclassical tearing modes (NTMs) [26]. As expected at the applied heating power and $q_{\min} < \frac{3}{2}$, NTMs also occur in the high-β_{pol} plasmas. A wavelet plot together with a time trace of the plasma energy is shown in Fig. 4. The discharge presented in Fig. 4 is equivalent to the one in Fig. 1, except for a lower NBI power of 7.5 MW. We start with an Ohmic phase and sawtooth activity, and later, with NBI, the sawteeth disappear and $(m = 1, n = 1)$ fish-bones develop similar to the improved H-mode discharges [9]. At $t = 2.45$ s a $(m = 3, n = 2)$ NTM occurs, most probably triggered by a fish-bone acting as a seed island. Because of the high q_{95} and the small island width the mode amplitude and the corresponding energy reduction remain comparatively small ($\delta W = 18$ kJ compared to 300 kJ of total plasma energy). Furthermore the mode activity vanishes after some time and the plasma energy recovers. The small energy reduction is to some extent expected because the position of the $q = 1.5$ surface at high q_{95} is closer to the plasma center ($\rho_{\text{tor}} = 0.26$ compared to $\rho_{\text{tor}} = 0.55$ at $q_{95} = 4$) and thus the plasma volume affected by the NTM is smaller.

Figure 5 shows the q and current profiles and their different components as calculated by neoclassical current diffusion and bootstrap current [27] using the ASTRA transport code. Also, for comparison, the profiles inferred from the equilibrium reconstruction based on MSE measurements are presented. Inside $\rho_{\text{tor}} = 0.08$ the measurements are not available, indicated by the dotted line. The current diffusion calculation is started at $t = 0.2$ s. At about $t = 1$ s the loop voltage is spatially almost constant which means that the starting conditions do not strongly influence the resulting current profile. After the heating power ramp, the plasma is again in a nonstationary state (mostly because the bootstrap current depends on the current profile itself, providing a kind of feedback loop) until the discharge ends. The contribution of the Ohmic current of $I_{\text{OH}} = 25$ kA is negligible. The main parts are the neutral beam driven

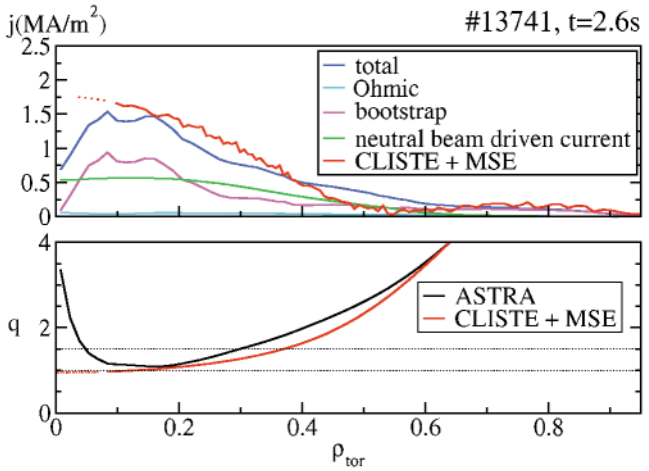

FIG. 5 (color). In the upper part, the current profile as derived from the transport code ASTRA and from an equilibrium reconstruction by CLISTE using MSE measurements is presented. In the lower part of the figure the corresponding q profiles are shown.

current of $I_{\mathrm{NBI}} = 166$ kA, which is broad but peaked towards the the plasma center, and the bootstrap current of $I_{\mathrm{BS}} = 200$ kA with the main contribution in the plasma core. The shape of the total current profile is dominated by the bootstrap current and is in agreement with the one derived from MSE. At the very center of the plasma the calculations predict strong shear reversal, caused by the drop of the bootstrap current down to zero as the gradients of temperature and density become zero. This feature cannot be resolved by the MSE diagnostic. In agreement with the MSE results the $(1, 1)$ fish-bone activity suggests the presence of a $q = 1$ surface. The existence of the strong reversed shear in the plasma core is still unclear because no measurement is available and the standard neoclassical theory breaks down in the plasma core because the trapped particle orbits become large compared to the gradient lengths. But it has some influence on the calculation of the bootstrap current near the plasma core.

In summary, discharges with high β_{pol} and an internal transport barrier at $\bar{n}_e/n^{\mathrm{gr}} \approx 1$ have been produced. Up to now only a few discharges in the high-β_{pol} regime have been produced in ASDEX Upgrade but they are easily reproducible, mainly because they already start from stationary conditions, as they do not require auxiliary heating during the current ramp-up for q profile shaping. Transiently, full noninductive current drive has been demonstrated based on high beam and bootstrap current fractions. Calculations of the ITG mode stability suggest that the favorable transport properties are generated by the neoclassical poloidal plasma rotation which is proportional to the ion temperature gradient. Although $q_{\mathrm{min}} < 1.5$, NTMs do not limit the confinement at 10 MW of NBI. Future investigations will concentrate on the enhancement of the bootstrap current by off-axis neutral beam current drive (NBCD). The modification of one of the ASDEX Upgrade neutral beam injectors is near completion with an off-axis current drive capability of up to 250 kA. First calculations including the off-axis NBCD show that in addition to the beam current the bootstrap current increases due to the effect of the local poloidal magnetic field reduction. This would offer the extension of the operating regime to higher plasma currents while maintaining the improved plasma properties.

[1] F. Wagner *et al.,* Phys. Rev. Lett. **49**, 1408 (1982).
[2] A. M. Messiaen *et al.,* Phys. Rev. Lett. **77**, 2487 (1996).
[3] M. Greenwald *et al.,* Nucl. Fusion **28**, 2199 (1988).
[4] Y. Koide *et al.,* Phys. Rev. Lett. **72**, 3662 (1994).
[5] S. Günter *et al.,* Phys. Rev. Lett. **84**, 3097 (2000).
[6] C. Gormezano *et al.,* Phys. Rev. Lett. **80**, 5544 (1998).
[7] F. M. Levinton *et al.,* Phys. Rev. Lett. **75**, 4417 (1995).
[8] E. J. Strait *et al.,* Phys. Rev. Lett. **75**, 4421 (1995).
[9] O. Gruber *et al.,* Phys. Rev. Lett. **83**, 1787 (1999).
[10] B. W. Rice *et al.,* Nucl. Fusion **39**, 1855 (1999).
[11] F. X. Söldner *et al.,* Nucl. Fusion **34**, 985 (1994).
[12] T. C. Luce *et al.,* Phys. Rev. Lett. **83**, 4550 (1999).
[13] C. C. Petty *et al.,* Nucl. Fusion **35**, 773 (1995).
[14] T. Oikawa *et al.,* Nucl. Fusion **40**, 435 (2000).
[15] O. Sauter, C. Angioni, and Y. R. Lin-Liu, Phys. Plasmas **6**, 2834 (1999).
[16] Y. Kamada *et al.,* Nucl. Fusion **39**, 1845 (1999).
[17] T. Ozeki *et al.,* Nucl. Fusion **35**, 861 (1995).
[18] P. J. McCarthy, P. Martin, and W. Schneider, Max-Planck-Institut für Plasmaphysik, IPP Report No. 5/85, 1999 (unpublished).
[19] R. C. Wolf, P. J. McCarthy, F. Mast, and H. P. Zehrfeld, Europhys. Conf. Abstr. **21A**, 1509 (1997).
[20] A. Stäbler *et al.,* Europhys. Conf. Abstr. **23J**, 1437 (1999).
[21] A. B. Hassam, T. M. Antonsen, J. F. Drake, and P. N. Guzdar, Phys. Fluids B **2**, 1822 (1990).
[22] A. G. Peeters, Report No. IAEA-CN-77/EXP5/O6, 2000 (unpublished).
[23] Y. B. Kim, P. H. Diamond, and R. J. Groebner, Phys. Fluids B **3**, 2050 (1991).
[24] H. Meister, A. Kallenbach, A. G. Peeters, A. Kendl, J. Hobirk, and S. D. Pinches, "Measurement of Poloidal Flow, Radial Electric Field and $E \times B$ Shearing Rates at ASDEX Upgrade," Nucl. Fusion (to be published).
[25] R. E. Waltz *et al.,* Phys. Plasmas **4**, 2482 (1997).
[26] S. Günter *et al.,* Nucl. Fusion **39**, 1793 (1999).
[27] W. A. Houlberg, K. C. Shaing, S. P. Hirshman, and M. C. Zarnstorff, Phys. Plasmas **4**, 3230 (1997).